Ab initio potential-energy surface and rovibrational states of the HCN–HCl complex

Ad van der Avoird[a)]
Institute of Theoretical Chemistry, IMM, Radboud University Nijmegen, Toernooiveld 1, 6525 ED Nijmegen, The Netherlands

Thomas Bondo Pedersen[b)]
Department of Theoretical Chemistry, Chemical Center, University of Lund, P.O. Box 124, S-221 00 Lund, Sweden

Guillaume S. F. Dhont[c)]
Institute of Theoretical Chemistry, IMM, Radboud University Nijmegen, Toernooiveld 1, 6525 ED Nijmegen, The Netherlands

Berta Fernández
Department of Physical Chemistry, Faculty of Chemistry, University of Santiago de Compostela, E-15782 Santiago de Compostela, Spain

Henrik Koch
Department of Chemistry, Norwegian University of Science and Technology, N-7491 Trondheim, Norway

(Received 2 February 2006; accepted 4 April 2006; published online 25 May 2006)

A four-dimensional intermolecular potential-energy surface has been calculated for the HCN–HCl complex, with the use of the coupled cluster method with single and double excitations and noniterative inclusion of triples. Data for more than 13 000 geometries were represented by an angular expansion in terms of coupled spherical harmonics; the dependence of the expansion coefficients on the intermolecular distance R was described by the reproducing kernel Hilbert space method. The global minimum with $D_e=1565\ \mathrm{cm}^{-1}$ and $R_e=7.47a_0$ has a linear HCN–HCl hydrogen-bonded structure with HCl as the donor. A secondary hydrogen-bonded equilibrium structure with $D_e=564\ \mathrm{cm}^{-1}$ and $R_e=8.21a_0$ has a T-shaped geometry with HCN as the donor and the acceptor HCl molecule nearly perpendicular to the intermolecular axis. This potential surface was used in a variational approach to compute a series of bound states of the isotopomers HCN–H^{35}Cl, DCN–H^{35}Cl, and HCN–H^{37}Cl for total angular momentum $J=0,1,2$ and spectroscopic parities e, f. The results could be analyzed in terms of the approximate quantum numbers of a linear polyatomic molecule with two coupled bend modes, plus a quantum number for the intermolecular stretch vibration. They are in good agreement with the recent high resolution spectrum of Larsen *et al.* [Phys. Chem. Chem. Phys. **7**, 1953 (2005)] in the region of 330 cm^{-1} corresponding to the HCl libration. The (partly anomalous) effects of isotopic substitutions on the properties of the complex were explained with the aid of the calculations.
 [DOI: 10.1063/1.2200345]

I. INTRODUCTION

The study of weak intermolecular interactions has evolved into a discipline in which theoretical calculations and experimental spectroscopy are inextricably linked. Since highly accurate *ab initio* calculations have become feasible, theoretical calculations may facilitate, or even make possible, the experimental assignment of intermolecular rovibrational transitions. One example is Ar–CO, a prototype van der Waals complex, for which numerous theoretical and experimental studies (see, e.g., Refs. 1–3 and references therein) have led to a nearly complete understanding of the lower-lying intermolecular rovibrational levels.

As one of the smallest hydrogen-bonded dimers the HCN–HCl complex seems ideal for *ab initio* quantum chemical studies including electron correlation. To date, however, only one such study has appeared. In 1998, Araújo and Ramos[4] presented a second-order Møller-Plesset[5] (MP2) study of the equilibrium geometries, binding energies, and vibrational properties of the HCN–HX (X=F,Cl,NC,CN,CCH) series of dimers. Although Ref. 4 is mainly focused on the changes in monomer properties on formation of the complex, harmonic vibrational frequencies are given for the intermolecular stretch and bend modes. However, as the intermolecular modes are large amplitude motions, the harmonic approximation cannot be expected to give accurate results, certainly not for the overtones.

A possible reason for the little theoretical interest in the HCN–HCl complex could be the scarcity of experimental results on the intermolecular motion. The HCN–HCl dimer

a)Electronic mail: A.vanderAvoird@theochem.ru.nl
b)Electronic mail: Thomas.Pedersen@teokem.lu.se
c)Present address: Université du Littoral, MREI2, LPCA, UMR CNRS 8101, 189a av. Maurice Schumann, 59140 Dunkerque, France

was first observed in the gas phase by Legon *et al.*[6] who determined accurate spectroscopic constants for the ground state and deduced that HCN–HCl is linear with a vibrationally averaged distance of 3.9380 Å between the centers of mass of the monomers. Bender *et al.*[7] and Block and Miller[8] later observed a small redshift (2.5 cm^{-1}) of the intramolecular CH stretch vibration upon dimerization, and Bender *et al.*[7] estimated the level origins of the HCN libration (intermolecular bend vibration) and the intermolecular stretch vibration to be 41 and 100 cm^{-1}, respectively. Larsen *et al.*[9] observed a sizable redshift (107 cm^{-1}) of the intramolecular HCl stretching vibration on dimerization. Recently, using a synchrotron radiation source to access the difficult far-infrared spectral region, the first direct observation of the intermolecular HCl libration was reported by Larsen *et al.*[10] This band appears to have its origin at 331 cm^{-1}. These authors also observed a number of hot bands involving anharmonic coupling of the HCN and HCl librations.

Although the harmonic results of Araújo and Ramos[4] (53, 115, and 312 cm^{-1} for the HCN libration, intermolecular stretch, and HCl libration, respectively) are in reasonable agreement with the experimental frequencies, we believe that a more thorough *ab initio* study of the HCN–HCl complex is called for. In the present paper we present results obtained from a full four-dimensional intermolecular potential-energy surface (PES) computed with the highly correlated coupled cluster singles and doubles with perturbative triples [CCSD(T)] method.[11]

II. POTENTIAL-ENERGY SURFACE

A. *Ab initio* calculations

The HCN–HCl dimer is here treated as a van der Waals complex with large amplitude motions and Jacobi coordinates are used to describe the geometry of the complex. Both the HCN and HCl monomers are treated as rigid rotors, which implies that we neglect the weak coupling of the intermolecular vibrations to the intramolecular modes that have much higher frequencies. HCN is linear with CH and CN bond lengths of 1.062 36 and 1.156 79 Å,[12] respectively. The HCl bond length was fixed at 1.2838 Å.[13] The potential-energy surface depends on four coordinates: R, θ_{HCN}, θ_{HCl}, and ϕ. The coordinate R is the length of the intermolecular vector $\mathbf{R}$ which points from the center of mass of the HCN molecule to the center of mass of HCl. The atomic masses are 1.007 825 03 amu for H, 12 amu for C, 14.003 074 amu for N, and 34.968 85 27 amu for ^{35}Cl. The coordinate θ_{HCN} is the angle between the vector $\mathbf{R}$ and the HCN monomer axis pointing from N to H, while θ_{HCl} is the angle between $\mathbf{R}$ and the HCl axis pointing from Cl to H. Both angles range from 0 to π. The ϕ coordinate is the dihedral angle between the planes through the vector $\mathbf{R}$ and the two monomer axes. This angle takes values between $-\pi$ and π.

Space inversion, which is the only feasible symmetry operation[14] in the permutation-inversion group of the HCN–HCl complex, is equivalent to reflection in the xz plane of a body-fixed frame with the z axis along the vector $\mathbf{R}$. It changes the internal coordinate ϕ into $-\phi$. This symmetry reduces the computational effort because only points with ϕ between 0 and π are needed to obtain the complete potential surface.

A grid of points on the intermolecular PES is computed at the CCSD(T) level of theory using Dunning's correlation consistent polarized valence triple-zeta basis set augmented with diffuse functions (aug-cc-pVTZ).[15–17] The core orbitals ($1s$ on carbon and nitrogen; $1s$, $2s$, and $2p$ on chlorine) are frozen in the correlation treatment and we employ the Boys-Bernardi counterpoise correction[18] to account for the basis set superposition error (BSSE). The PES grid is obtained by varying the four coordinates as follows. R takes values from $5.0a_0$ to $10.0a_0$ in steps of $0.5a_0$. In addition, interaction energies are computed at $R=12.0a_0$, $14.0a_0$, $16.0a_0$, and $20.0a_0$. The angles θ_{HCN} and θ_{HCl} take values between 0 and π in steps of $\pi/12$ (15°). The dihedral angle ϕ is varied between 0 and π in steps of $\pi/6$ (30°). Removing redundancies, we arrive at a total grid size of 13 425 points on the PES. The *ab initio* calculation of the PES grid is carried out with the DALTON electronic structure program.[19]

It is well known (see, e.g., Ref. 1) that a small set of additional basis functions located at the middle of the intermolecular bond can significantly speed up basis set convergence of the interaction energy. In the present case, however, we encountered severe problems in converging the Hartree-Fock and coupled cluster equations when such functions were included. These problems typically emerged at large intermolecular separations, in some cases also when bond functions were not included. We therefore decided to proceed without bond functions. Close to the global minimum of the PES bond functions do not present computational problems. At the linear HCN–HCl geometry with $R=7.50a_0$, we compute the CCSD(T) interaction energy to be −1560.3 and −1532.9 cm^{-1} using the aug-cc-pVTZ basis set with and without the $3s3p2d1f1g$ set of midbond functions from Ref. 20, respectively. Hence, at this geometry the midbond functions increase the absolute value of the interaction energy by 1.8%.

B. Analytic representation of the potential surface

The PES is represented by the following expansion in internal (or body-fixed) dimer coordinates:

$$V(R,\theta_A,\theta_B,\phi)=\sum_{L_A,L_B,L} v_{L_A,L_B,L}(R)A_{L_A,L_B,L}(\theta_A,\theta_B,\phi), \quad (1)$$

with coefficients $v_{L_A,L_B,L}(R)$ depending on R. The angular functions with $\theta_A \equiv \theta_{\mathrm{HCN}}$ and $\theta_B \equiv \theta_{\mathrm{HCl}}$ are defined as

$$\begin{aligned} &A_{L_A,L_B,L}(\theta_A,\theta_B,\phi) \\ &\quad=\sum_{M=-\min(L_A,L_B)}^{\min(L_A,L_B)} \begin{pmatrix} L_A & L_B & L \\ M & -M & 0 \end{pmatrix} \\ &\qquad\times C_{L_A,M}(\theta_A,\phi_A)C_{L_B,-M}(\theta_B,\phi_B) \\ &\quad=\sum_{M=0}^{\min(L_A,L_B)} (-1)^M \begin{pmatrix} L_A & L_B & L \\ M & -M & 0 \end{pmatrix} A_{L_A,L_B,M}(\theta_A,\theta_B,\phi), \end{aligned} \quad (2)$$

where $C_{L,M}(\theta,\phi)$ are Racah-normalized spherical harmonics, and the difference between the azimuthal angles of the two monomers is the dihedral angle $\phi=\phi_A-\phi_B$. The "primitive" angular functions are

$$A_{L_A,L_B,M}(\theta_A,\theta_B,\phi)=P_{L_A,M}(\cos\theta_A)P_{L_B,M}(\cos\theta_B)\cos M\phi, \tag{3}$$

where $P_{L,M}(\cos\theta)$ are Schmidt seminormalized associated Legendre functions given, for example, in Eq. (9) of Ref. 21. It is also possible, of course, to expand the potentials directly in terms of the primitive functions

$$V(R,\theta_A,\theta_B,\phi)=\sum_{L_A,L_B,M} v_{L_A,L_B,M}(R)A_{L_A,L_B,M}(\theta_A,\theta_B,\phi). \tag{4}$$

We will briefly call this the *LLM* expansion, while Eq. (1) will be called the *LLL* expansion. The *LLL* expansion has the advantage that the coefficients $v_{L_A,L_B,L}(R)$ are invariant under rotation of the coordinate frame. Hence, this expansion can easily be transformed to space-fixed coordinates.

Both expansions are in terms of orthogonal angular functions, and therefore each expansion (or Fourier) coefficient $v_{L_A,L_B,M}(R)$ or $v_{L_A,L_B,L}(R)$ can be looked upon as an overlap integral between the expansion function $A_{L_A,L_B,M}(\theta_A,\theta_B,\phi)$ or $A_{L_A,L_B,L}(\theta_A,\theta_B,\phi)$ and the function to be expanded. This implies that the expansion coefficients can be obtained by numerical integration on a Gauss-Legendre quadrature grid for the angles θ_A, θ_B, and an evenly spaced grid for ϕ. For the *LLL* expansion the number of ϕ grid points must at least be equal to the smallest of the numbers of θ_A and θ_B grid points, which numbers must at least be equal to $\max(L_A)+1$ and $\max(L_B)+1$. For the coefficients of the *LLM* expansion of Eq. (4) the integrals over θ_A, θ_B, and ϕ can be carried out independently. The required number of ϕ grid points, $\max(M)+1$, is smaller than the number of θ_A and θ_B points when the range of M is restricted to be smaller than $\min(L_A,L_B)$. Moreover, the *LLM* expansion is computationally less expensive due to the absence of the summation over M and of the $3j$ symbol in the primitive functions of Eq. (3).

Since for the smallest values of R the potential becomes extremely repulsive for certain orientations of the monomers one would need terms with very high values of L_A and L_B in the expansion. To avoid this, the potential was damped in these strongly repulsive regions by means of a hyperbolic tangent function up to a value $V_{\max}$, as in Ref. 22

$$\tilde{V}=\begin{cases} V, & \text{for } V\leqslant V_0 \\ V_0+\beta^{-1}\tanh[\beta(V-V_0)], & \text{for } V>V_0, \end{cases} \tag{5}$$

where $\beta\equiv[V_{\max}-V_0]^{-1}$. With this scheme, the damped potential $\tilde{V}$ is continuous around V_0 up to the second derivative. Care was taken to use sufficiently high values of V_0 and $V_{\max}$, so that the potential was affected only in regions that are not of any practical importance in bound-state calculations. The actual values used were $V_0=20\,000\ \mathrm{cm}^{-1}$, and $V_{\max}=2V_0$.

After some experimentation with direct least-squares fitting of the expansion to the *ab initio* points, which produced less accurate results, we developed the following procedure. For each value of R on the *ab initio* grid we evaluated the coefficients $v_{L_A,L_B,M}(R)$ in the *LLM* expansion by numerical quadrature of the "overlap integral" of the expansion function $A_{L_A,L_B,M}(\theta_A,\theta_B,\phi)$ and the potential $V(R,\theta_A,\theta_B,\phi)$. For each of the seven equally spaced *ab initio* grid points ϕ, the potential was first obtained on a 12×11 Gauss-Legendre integration grid in θ_A,θ_B by means of a two-dimensional cubic spline interpolation of the 13×13 evenly spaced *ab initio* points (θ_A,θ_B). This interpolation method is encoded in the INTERP2 function of the MATLAB program package.[23] In order to avoid the uncertainty about the first derivatives that occurs in a cubic spline method at the boundaries of the interval to be interpolated we extended the range of θ_A and θ_B from $0\leqslant\theta\leqslant\pi$ to $-\pi\leqslant\theta\leqslant2\pi$. The values of the potentials for $-\pi\leqslant\theta\leqslant0$ and for $\pi\leqslant\theta\leqslant2\pi$ were obtained from the original values for $0\leqslant\theta\leqslant\pi$ by means of the transformations

$$\begin{aligned} V(R,\theta_A,\theta_B,\phi)&=V(R,2\pi-\theta_A,\theta_B,\pi+\phi)\\ &=V(R,\theta_A,2\pi-\theta_B,\pi+\phi), \end{aligned} \tag{6}$$

which are simply a consequence of the periodic boundary conditions in spherical polar coordinates. In addition, we used that $V(R,\theta_A,\theta_B,\phi)=V(R,\theta_A,\theta_B,-\phi)$, which follows from the reflection symmetry mentioned in Sec. II A. This extension turned out to be particularly important for the HCN–HCl system, because the rather steep global minimum occurs for a linear geometry with $\theta_A=\pi$ and $\theta_B=\pi$, i.e., at the corner of the "normal" interval with $0\leqslant\theta_A,\theta_B\leqslant\pi$. The coefficients $v_{L_A,L_B,M}(R)$ were thus computed for all values $0\leqslant L_A\leqslant11$, $0\leqslant L_B\leqslant9$, and $0\leqslant M\leqslant6$.

Once the coefficients $v_{L_A,L_B,M}(R)$ in the *LLM* expansion were obtained, the coefficients $v_{L_A,L_B,L}(R)$ in the *LLL* expansion were computed from the equation

$$\begin{aligned} v_{L_A,L_B,L}(R)=(2L+1)&\sum_{M=0}^{\min(L_A,L_B)}(-1)^M(2-\delta_{M0})\\ &\times\begin{pmatrix} L_A & L_B & L \\ M & -M & 0 \end{pmatrix} v_{L_A,L_B,M}(R). \end{aligned} \tag{7}$$

This equation follows from the "inversion" of Eq. (2), with the use of the known properties of $3j$ symbols.[24] The expansion coefficients $v_{L_A,L_B,L}(R)$ vanish unless L_A+L_B+L is even. It should be noted that for given L_A and L_B, the number of L values with even L_A+L_B+L and $|L_A-L_B|\leqslant L\leqslant L_A+L_B$ is equal to the number of M values with $0\leqslant M\leqslant\min(L_A,L_B)$.

Finally, the angular expansion coefficients $v_{L_A,L_B,L}(R)$ were fitted as functions of R by means of the reproducing kernel Hilbert space (RKHS) method[25,26] with the reproducing kernel for distancelike variables. The dominant ($\propto R^{-3}$) contribution to the potential in the long range is given by the dipole-dipole interaction with $L_A=L_B=1$ and $L=2$. All contributions with $L=L_A+L_B$ and $L<5$, which decay slower than the leading induction and dispersion terms $\propto R^{-6}$, were fitted with RKHS parameter $m=L_A+L_B$, so that they decay as $R^{-L_A-L_B-1}$ beyond the outermost grid point.[25,26] All expansion coefficients with $L\neq L_A+L_B$ or $L_A+L_B+1\geqslant6$ were fitted with RKHS parameter $m=5$ and decay as R^{-6} for very large

TABLE I. Multipole moments of HCN and HCl in atomic units $e(a_0)^L$, from CCSD(T) calculations with aug-cc-pVTZ basis, see text, defined with the molecules oriented along the z axis, the origin at the center of mass, and the H atoms on the positive side. Literature values are given in parentheses.

L	Q_0^L	
HCN		
1	1.1821	(1.187,[a] 1.1648,[b] 1.1800[c])
2	1.6817	(2.3,[d] 1.6235,[b] 1.6461[c])
3	9.7902	(9.762[c])
HCl		
1	0.4289	(0.4301,[e] 0.4238,[f] 0.4443[g])
2	2.7126	(2.78,[h] 2.67,[f] 2.6972[g])
3	4.0200	(3.94,[f] 3.9537[g])

[a]Experimental value (Ref. 36).
[b]From MP4 calculations (Ref. 37).
[c]From CCSD(T) calculations (Ref. 38).
[d]Experimental value (Ref. 39).
[e]Experimental value (Ref. 40).
[f]From CCSD(T) calculations (Ref. 41).
[g]From multireference configuration interaction calculations (MRCI) (Ref. 35).
[h]Experimental value (Ref. 42).

R. The smoothness parameter n was always 2. The mean absolute deviation between the analytic representation and the *ab initio* values is about 1.1% at $R=6a_0$, 1.8% at $R=7a_0$, and about 0.3% for $R \geqslant 8a_0$, relative to the mean absolute value of the potential at the same distance. The FORTRAN code of the analytic potential is available from the authors upon request.

C. Multipole expansion of the electrostatic interaction energy

We also computed the potential V in the long range directly from the multipole expansion. It was already shown in Ref. 27 that this expansion takes the form of Eq. (1) with the expansion coefficients of the first order electrostatic energy given by

$$v_{L_A L_B L}(R) = \delta_{L_A+L_B,L}(-1)^{L_B}\begin{pmatrix} 2L_A+2L_B \\ 2L_A \end{pmatrix}^{1/2} \times Q_0^{L_A} Q_0^{L_B} R^{-L_A-L_B-1}. \quad (8)$$

The spherical multipole moments $Q_0^{L_A}$ of HCN and $Q_0^{L_B}$ of HCl were calculated at the (frozen core) CCSD(T)/aug-cc-pVTZ level with the ACES II program.[28] The values obtained are listed in Table I. The leading term in this expansion is the dipole-dipole term $\propto R^{-3}$ and the expansion contains terms up to R^{-7}, inclusive, but only the terms up to R^{-5} inclusive are complete.

III. CALCULATION OF ROVIBRATIONAL STATES

The vector $\mathbf{R}$ has the spherical polar angles (β,α) with respect to a space-fixed frame. Rotation of the space-fixed frame over the angles β around the y axis and α around the z axis leads to a body-fixed (two-angle embedded) dimer frame which has $\mathbf{R}$ along its z axis. The vectors $\mathbf{r}_A$ and $\mathbf{r}_B$ along the monomer axes are expressed with respect to this two-angle embedded dimer frame.

The bound states of the HCN–HCl dimer were computed by diagonalizing the Hamiltonian,

$$H = B_{\mathrm{HCN}}\mathbf{j}_A^2 + B_{\mathrm{HCl}}\mathbf{j}_B^2 - \frac{\hbar^2}{2\mu_{AB}R}\frac{\partial^2}{\partial R^2}R + \frac{\mathbf{J}^2+|\mathbf{j}_A+\mathbf{j}_B|^2-2(\mathbf{j}_A+\mathbf{j}_B)\cdot\mathbf{J}}{2\mu_{AB}R^2} + V. \quad (9)$$

Here $B_{\mathrm{HCN}}=1.4784\ \mathrm{cm}^{-1}$ and $B_{\mathrm{H}^{35}\mathrm{Cl}}=10.4402\ \mathrm{cm}^{-1}$ are the experimental ground-state rotational constants of the monomers.[29,30] The quantity μ_{AB} is the reduced mass of the dimer, $\mathbf{J}$ is the total angular momentum, and $\mathbf{j}_A$, $\mathbf{j}_B$ are angular momenta of the monomers. The potential $V \equiv V(R,\theta_A,\theta_B,\phi)$ was described in Sec. II. This Hamiltonian is represented in the following basis:

$$|n(j_A j_B)j_{AB}K;JM\rangle = |n\rangle|(j_A j_B)j_{AB}K;JM\rangle, \quad (10)$$

with the normalized angular basis functions given by

$$|(j_A j_B)j_{AB}K;JM\rangle = \sqrt{\frac{2J+1}{4\pi}}D_{MK}^{(J)}(\alpha,\beta,0)^* \times \sum_{m_A m_B} Y_{m_A}^{(j_A)}(\hat{\mathbf{r}}_A)Y_{m_B}^{(j_B)}(\hat{\mathbf{r}}_B)\langle j_A m_A j_B m_B|j_{AB}K\rangle. \quad (11)$$

Here $Y_{m_X}^{(j_X)}(\hat{\mathbf{r}}_X)$ denote spherical harmonics of the body-fixed angles of monomer X, which are coupled with Clebsch-Gordan (CG) coefficients[24] $\langle j_A m_A j_B m_B|j_{AB}K\rangle$. The quantity $D_{MK}^{(J)}(\alpha,\beta,0)^*$ is a Wigner rotation function.[24] The total angular momentum J and its space-fixed z component M are exact quantum numbers. The quantum number K, which gives the projection of $\mathbf{J}$ (and of $\mathbf{j}_A+\mathbf{j}_B$) on the dimer body-fixed z axis $\mathbf{R}$, is almost conserved. Functions with different K are mixed only by the J_+ and J_- shift terms in the Coriolis interaction $2(\mathbf{j}_A+\mathbf{j}_B)\cdot\mathbf{J}$.

The radial basis functions are given by $|n\rangle \equiv \chi_n(R)/R$, where the $\chi_n(R)$ are eigenfunctions of a reference Hamiltonian,

$$H^{\mathrm{ref}} = -\frac{\hbar^2}{2\mu_{AB}}\frac{\partial^2}{\partial R^2} + V^{\mathrm{ref}}(R). \quad (12)$$

The χ_n were computed using a sinc-function discrete variable representation[31] (DVR) on a 210-point R grid equally spaced in the range from $5a_0$ to $20a_0$. The reference potential $V^{\mathrm{ref}}(R)$ was obtained from a cut of the full potential $V(R,\theta_A,\theta_B,\phi)$ with the angles (θ_A,θ_B) fixed at their equilibrium values (π,π). This cut was scaled in order to achieve a nonlinear optimization of the radial basis and a term linear in R was added to include the effect of continuum wave functions. Both the scaling factor of 0.5 and the slope of $165\ \mathrm{cm}^{-1}/a_0$ of the linear term in $V^{\mathrm{ref}}(R)$ were optimized by minimization of the ground-state energy and the lower excited levels of the HCN–HCl complex in a full four-dimensional calculation with a smaller basis. The final vibrational basis $|n\rangle$ contained the first 22 eigenfunctions of H^{ref}.

The potential is strongly anisotropic and rather high values of the angular quantum numbers j_A and j_B in the basis had to be included to converge the energy levels. All of the

results reported were obtained with an angular basis of maximum $j_A=14$ and $j_B=12$. The increase of the maximum HCN internal rotation quantum number j_A from 13 to 14 still lowered the ground-state energy by 0.07 cm^{-1}, the fundamental HCN and HCl librational frequencies were changed by less than 0.1%. The increase of the maximum HCl quantum number j_B from 11 to 12 lowered the ground-state level by 0.22 cm^{-1} and changed the librational frequencies by less than 1%. The very small l-doubling constant q of the librational modes, which is on the order of 10^{-4} cm^{-1} (see below), is nearly unchanged by the increase of the maximum j_B from 11 to 12, but changes by 20%–30% by the increase of the maximum j_A from 13 to 14. Also the small isotope shifts of the librational frequencies (on the order of 0.2–0.01 cm^{-1}, see below) are still expected to change with an increase of the basis size. We kept exactly the same basis and radial grid in all calculations in order to minimize the error in the relative quantities.

The HCN–HCl dimer has a permutation-inversion (PI) group which contains only two elements: the identity E and space inversion E^*. The two irreducible representations (irreps) that are symmetric and antisymmetric under E^* are denoted by A' and A'', respectively. For the interpretation of the results it is more illustrative to label the states with their spectroscopic parity ϵ (e or f) which is related to the parity p under E^* as $p=\epsilon(-1)^J$. The overall parity p reflects the symmetry of the total wave function including rotation, while the spectroscopic parity e or f reflects the symmetry of the wave function corresponding to the internal motion of the complex.

We calculated the rovibrational bound states of the dimer for total angular momentum $J=0$, 1, and 2 for both A' and A'' symmetry. The total basis size ranges from 17 732 functions for the $J=0$, A'' block up to 100 144 functions for the $J=2$, A' block. The 30 to 45 lowest eigenvectors of the Hamilton matrix were computed using a direct variant of the Davidson algorithm.[32,33]

Since Coriolis coupling was included in the calculation, K is, strictly speaking, not a good quantum number. Nevertheless, in most states the contribution of a single $|K|$ was dominant, enabling us to label the states unambiguously with $|K|$.

IV. DIFFERENT ISOTOPOMERS

Far-infrared spectra of various isotopomers of HCN–HCl were measured[10] in high resolution. $H^{12}CN$ was replaced by DCN and by $H^{13}CN$, while $H^{35}Cl$ is naturally accompanied by $H^{37}Cl$ in the ratio of 3 to 1. In order to compute the rovibrational states of these isotopomers from the same potential surface (described above) we had to proceed in a few steps. First the potential $V(R,\theta_A,\theta_B,\phi)$ must be re-expressed in a new set of Jacobi coordinates obtained by the shifts of the monomer centers of mass. The following formulas can be used for this purpose:

$$\hat{\mathbf{r}}_A\cdot\hat{\mathbf{r}}_B=\cos\theta_A\cos\theta_B+\sin\theta_A\sin\theta_B\cos\phi,$$

$$R'=[R^2-2\delta_A\delta_B\hat{\mathbf{r}}_A\cdot\hat{\mathbf{r}}_B-2\delta_A R\cos\theta_A+2\delta_B R\cos\theta_B+\delta_A^2+\delta_B^2]^{1/2},$$

$$\cos\theta_A'=\frac{R\cos\theta_A-\delta_A+\delta_B\hat{\mathbf{r}}_A\cdot\hat{\mathbf{r}}_B}{R'},$$

$$\cos\theta_B'=\frac{R\cos\theta_B-\delta_A\hat{\mathbf{r}}_A\cdot\hat{\mathbf{r}}_B+\delta_B}{R'},$$

$$\cos\phi'=\frac{\hat{\mathbf{r}}_A\cdot\hat{\mathbf{r}}_B-\cos\theta_A'\cos\theta_B'}{\sin\theta_A'\sin\theta_B'},\tag{13}$$

where δ_A and δ_B are the shifts of the centers of mass of monomers A and B along their respective z axes and the Jacobi coordinates R', θ_A', θ_B', and ϕ' are defined with respect to the new monomer origins.

Next the potential must be re-expanded in the set of angular functions $A_{L_A,L_B,L}(\theta_A',\theta_B',\phi')$ in these new Jacobi coordinates, cf. Eq. (1). The new expansion coefficients $v_{L_A,L_B,L}(R)$ were obtained by means of the numerical quadrature and transformation procedure described in Sec. II B. The potential was generated on the same type of three-dimensional angular quadrature grid as in Sec. II B by expressing the new Jacobi coordinates into the original ones by means of Eq. (13) and using the FORTRAN code of the analytic potential in the original coordinates. The number of grid points chosen was larger, however, and the values of L_A and L_B at which the expansion was truncated were larger than before, in order not to lose too much accuracy by this transformation procedure. The new grid contained 14 and 13 Gauss-Legendre points of θ_A and θ_B, respectively, and 13 equidistant points ϕ in the range from 0 to π. The maximum values of L_A and L_B in the new expansion were 13 and 11, and the maximum value of the intermediate quantum number M was 9. The deviation of the new expansion from the original one, when evaluated at the same HCN–HCl geometries, was typically a factor of 10 smaller than the deviation of the original expansion from the *ab initio* points.

Finally, the computation of the rovibrational levels of different isotopomers requires that one changes the atomic masses and the rotational constants of the monomers. The systems that we treated in addition to the original HCN–$H^{35}Cl$ complex were DCN–$H^{35}Cl$ and HCN–$H^{37}Cl$. The atomic masses are 2.014 101 778 amu for D and 36.965 902 6 amu for ^{37}Cl. The center of mass of HCN has shifted by $0.110\,12a_0$ in DCN and the mass center of $H^{35}Cl$ has shifted by $-0.003\,574\,1a_0$ in $H^{37}Cl$. The experimental ground-state rotational constants[29,30] of the isotopomers are $B_{DCN}=1.207\,75$ cm^{-1} and $B_{H^{37}Cl}=10.4245$ cm^{-1}.

V. RESULTS

A. Potential surface

A contour plot of the potential surface for planar geometries with $\phi=180°$ and 0° is shown in Fig. 1. The HCN–HCl distance R is optimized in this plot; the equilibrium

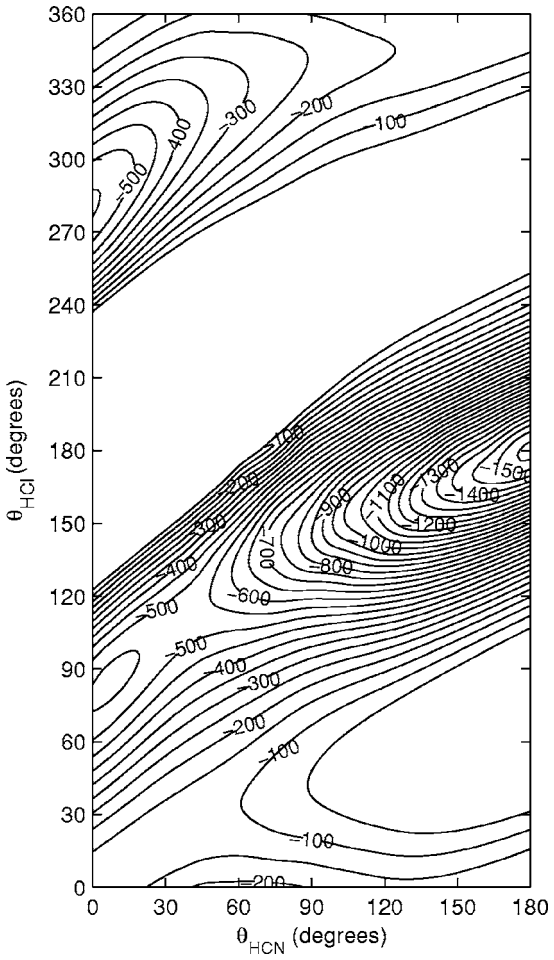

FIG. 1. Potential surface (in cm^{-1}) at planar geometries for optimized R. The lower half of the figure for $0° \leqslant \theta_{HCl} \leqslant 180°$ corresponds to $\phi=180°$, the upper half for $180° \leqslant \theta_{HCl} \leqslant 360°$ is obtained from the potential for $0° \leqslant \theta_{HCl} \leqslant 180°$ and $\phi=0°$ with the aid of the transformation in Eq. (6).

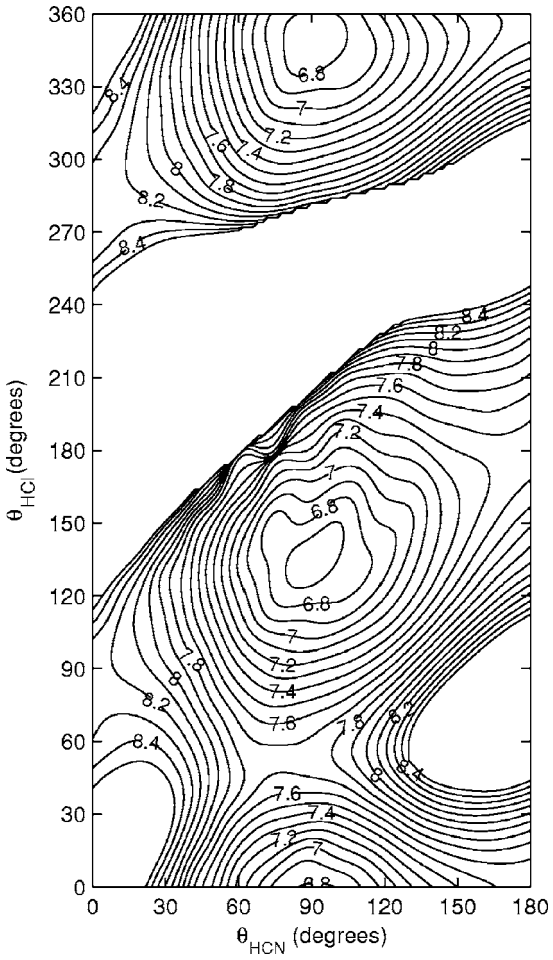

FIG. 2. Equilibrium values of R for the potential in Fig. 1 at planar geometries with $\phi=180°$ and $\phi=0°$, put together as described in Fig. 1.

values of R are plotted in Fig. 2. The global minimum in the potential with $D_e=1564.99\ cm^{-1}$ and $R_e=7.47a_0$ occurs for the linear HCN–HCl structure with HCl as the donor in the hydrogen bond and HCN as the acceptor ($\theta_{HCN}=180°$ and $\theta_{HCl}=180°$). A secondary hydrogen-bonded minimum with $D_e=564.10\ cm^{-1}$ and $R_e=8.21a_0$ is found at $\theta_{HCN}=7.9°$, $\theta_{HCl}=85.9°$, and $\phi=180°$. Here the HCN monomer is the donor in the hydrogen bond and HCl is the acceptor. When HCl is the hydrogen donor it is parallel to the intermolecular axis **R**, but when it is the acceptor it is nearly perpendicular to **R**. This was found also for HCl–HCl (Ref. 34) and OH–HCl.[35] The hydrogen-bonded structures of HCN–HCl that correspond to the global and local minimum in the potential are shown in Fig. 3.

The shortest bond distance R of less than $6.7a_0$ occurs for geometries with HCN nearly perpendicular to the bond axis **R** and HCl making an angle of about 135° with this axis, while $\phi=180°$. This geometry lies in the valley that connects the global and the local minimum. The latter is separated from the much deeper global minimum by a barrier of 36.6 cm^{-1} at $R=7.80a_0$, $\theta_{HCN}=34.8°$, $\theta_{HCl}=109.1°$, and $\phi=180°$.

In Fig. 4 one observes that the long-range electrostatic multipole-multipole interactions play an important role in the hydrogen bond. Especially in the global minimum at the linear HCN–HCl geometry, which is already the most stable structure if one considers only dipole-dipole interactions. The secondary minimum, with HCN as the hydrogen donor and HCl almost perpendicular to the hydrogen bond axis, is stabilized in particular by the interaction between the dipole of HCN and the quadrupole of HCl.

B. Bound states

The calculated binding energy D_0 of HCN–HCl equals 1091.35 cm^{-1}, and since the well depth of the potential is $D_e=1564.99\ cm^{-1}$ there is a substantial zero-point vibrational energy of 473.64 cm^{-1}.

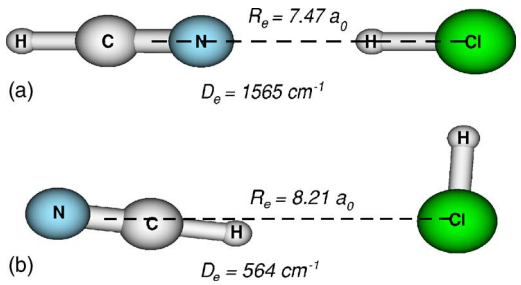

FIG. 3. (Color online) The two hydrogen bonded structures corresponding to minima in the potential surface. (a) Global minimum; (b) Local minimum.

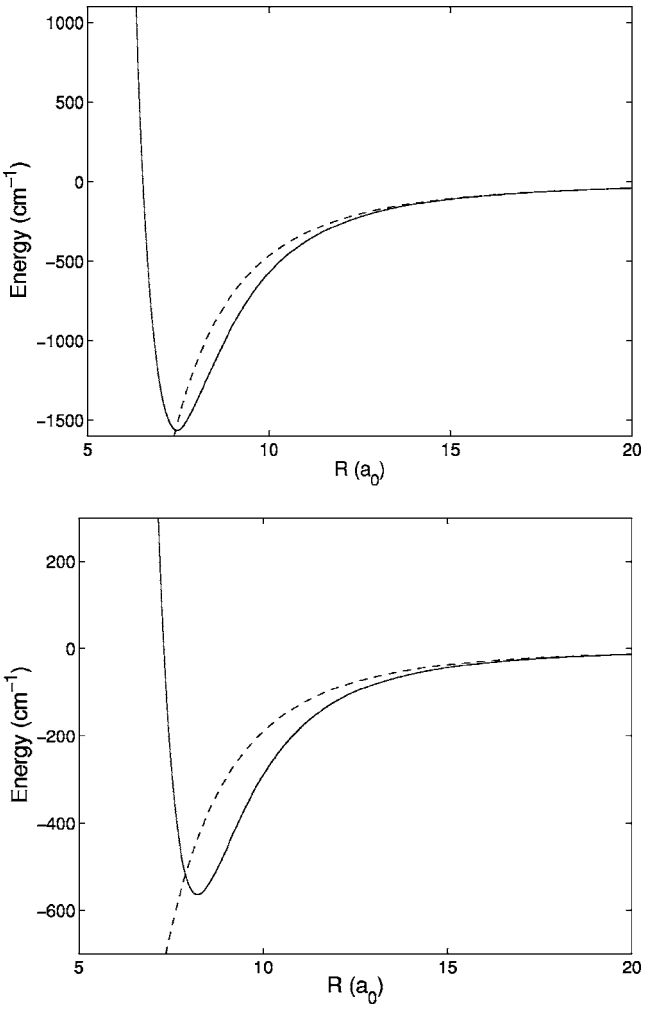

FIG. 4. Potential from the full CCSD(T) calculations (closed curves) and from the multipole expansion (dashed curves). The upper panel corresponds to the most stable linear HCN-HCl structure with $\theta_{\mathrm{HCN}}=180°$ and $\theta_{\mathrm{HCl}}=180°$, the lower panel to the secondary hydrogen-bonded minimum with $\theta_{\mathrm{HCN}}=8.0°$, $\theta_{\mathrm{HCl}}=86.0°$, and $\phi=180°$.

The bound levels computed on this potential surface are listed in Tables II–IV for $K=0$, $|K|=1$, and $|K|=2$, respectively. The approximate quantum number $|K|$ is nearly conserved and plays an important role, since it is directly related to the excitation of the HCN and HCl librations. In order to understand this, one might first look at Fig. 5, which shows that the ground-state wave function is quite well localized near the linear HCN–HCl equilibrium structure. The bend or librational mode(s) of a linear polyatomic molecule (or complex) are twofold degenerate and generate vibrational angular momentum, usually denoted by a quantum number l. Librational fundamentals with $v_b=1$ have $l=-1,1$, the first libration overtone with $v_b=2$ has $l=-2,0,2$, etc. In the present case, there are two such librators, characterized by the quantum numbers $v_{b\mathrm{HCN}}$ and $v_{b\mathrm{HCl}}$ with angular momenta l_{HCN} and l_{HCl}. The quantum number K, which is the projection of the total angular momentum J on the bond axis $\mathbf{R}$, is also the sum of the internal angular momenta of the bend modes, $K=l_{\mathrm{HCN}}+l_{\mathrm{HCl}}$. All the excited states in the energy region included in Tables II–IV are localized around the linear equilibrium geometry, as we shall illustrate below, and can therefore be characterized by these (approximate) quantum numbers. The other relevant quantum number, v_s, refers to the intermolecular stretch mode in the coordinate R.

The assignment of the quantum numbers to the levels in Tables II–IV is based on a characterization of the states in two ways. The first is an analysis of the eigenvectors in terms of the basis in Eqs. (10) and (11). The quantum numbers m_A and m_B in this basis correspond to the librational angular momenta l_{HCN} and l_{HCl}. In order to determine which values of m_A and m_B predominantly occur in a given eigenvector, we transform the coefficients in terms of the coupled basis of Eq. (11) to a set of coefficients in terms of an uncoupled basis consisting of products of spherical harmonics $Y_{m_A}^{(j_A)}(\hat{\mathbf{r}}_A)Y_{m_B}^{(j_B)}(\hat{\mathbf{r}}_B)$ and symmetric rotor functions $D_{MK}^{(J)}(\alpha,\beta,0)^*$. This "uncoupling" transformation is easy, since the Clebsch-Gordan coupling coefficients form an orthogonal matrix. The eigenvectors are either purely real or purely imaginary and therefore they are plus/minus combinations of basis functions with $\pm(m_A,m_B)$. The quantum numbers m_A and m_B are not strictly conserved, but in most of the eigenvectors a single pair of quantum numbers $(|m_A,m_B|)$ is clearly dominant. These correspond to the values of $|l_{\mathrm{HCN}}|$ and $|l_{\mathrm{HCl}}|$ in Tables II–IV. The relative sign of l_{HCN} and l_{HCl} can be derived from the value of $|K|$. The second characterization of the states is by plotting their wave functions; see Figs. 5–8. By looking at the nodes in these wave functions and considering the already known values of l_{HCN} and l_{HCl} it was not hard for most of the low-lying states to assign the quantum numbers $v_{b\mathrm{HCN}}$, $v_{b\mathrm{HCl}}$, and v_s. The values of the rotational constants B (discussed below) correlate well with the level of stretch excitation: higher v_s gives a smaller value of B.

The fundamental frequencies that we extract from these data are 48.7 cm^{-1} for the HCN libration and 311.7 cm^{-1} for the HCl libration. The stretch fundamental $(v_s=1)$ forms a Fermi resonance with the $l_{\mathrm{HCN}}=0$ component of the HCN libration overtone $v_{b\mathrm{HCN}}=2$. The frequency of 102.6 cm^{-1} for the intermolecular stretch mode is probably pushed up by this resonance, while the HCN libration overtone frequency of 84.2 cm^{-1} is lowered. The $l_{\mathrm{HCN}}=2$ component of the $v_{b\mathrm{HCN}}=2$ overtone level, which is not affected by this resonance, has a frequency of 94.4 cm^{-1}. This resonance repeats itself for $v_s=2$ and $v_{b\mathrm{HCN}}=4$, $v_s=3$ and $v_{b\mathrm{HCN}}=6$, etc. All of these states are strongly mixed, which complicated the analysis.

The levels were computed for total angular momentum $J=0$, 1, and 2. Just as in the analysis of the experimental spectra[10] the energy levels for $K=0$ were represented by the expression

$$E=\nu_0+BJ(J+1)-D_J J^2(J+1)^2. \tag{14}$$

The band origins ν_0, rotational constants B, and distortion constants D_J are included in Table II. The levels for $|K|=1$ are split by off-diagonal Coriolis interactions that mix the parity-adapted basis functions of $K=\pm 1$ with those of the same parity and $K=0$. The resulting small splitting between e and f parity levels is usually called l doubling. These levels were represented by the expression

TABLE II. Bound levels of HCN-H^{35}Cl for $K=0$: $J=0$ energies relative to the ground level with $D_0=1091.3529$ cm^{-1}, rotational constants B, and distortion constants D_J; all quantities in cm^{-1}. Levels labeled with a, b, and c are Fermi resonances; their quantum numbers v_s and $v_{b\mathrm{HCN}}$ are mixed.

v_s	$v_{b\mathrm{HCN}}$	$\lvert l_{\mathrm{HCN}}\rvert$	$v_{b\mathrm{HCl}}$	$\lvert l_{\mathrm{HCl}}\rvert$	Energy	B	$D_J\times10^6$
Parity e							
0	0	0	0	0	0.0000	0.06564	0.1137
0^a	2^a	0	0	0	84.1786	0.06693	0.2110
1^a	0^a	0	0	0	102.6006	0.06480	0.0421
0^b	4^b	0	0	0	161.8786	0.06882	0.3038
2^b	0^b	0	0	0	185.1942	0.06502	0.2464
1^b	2^b	0	0	0	203.3463	0.06519	−0.4195
0^c	6^c	0	0	0	236.6512	0.07057	0.5233
2^c	2^c	0	0	0	263.5679	0.06657	0.5277
3^c	0^c	0	0	0	279.1165	0.06458	−0.9534
1^c	4^c	0	0	0	301.8676	0.06245	−52.4258
		0	0	0	313.8570	0.07130	0.7276
		0	0	0	336.9295	0.06909	0.8640
0	1	1	1	1	352.2988	0.06560	−0.0002
		0	0	0	353.9780	0.06564	−23.0111
		0	0	0	368.8057	0.06471	−0.6098
		0	0	0	391.2631	0.07099	2.7800
Parity f							
0	1	1	1	1	352.1834	0.06566	0.1731
0	3	1	1	1	418.6330	0.06731	0.2719

$$E=\nu_0+(B\pm q/2)J(J+1), \tag{15}$$

where q is the l-doubling constant and the $+$ and $-$ signs hold for the f and e levels, respectively. These values are included in Table III. We could not extract a distortion constant D_J from these levels, because we only know their energies for $J=1$ and $J=2$. Finally, for the levels with $|K|=2$ we could not even derive rotational constants B, because we only computed energies for $J=2$ (which was already rather costly). The splitting between the $|K|=2$ levels of e and f parity is extremely small, because Coriolis coupling only mixes functions that differ by one in their values of K. Functions with $K=\pm2$ only mix indirectly (through $K=\pm1$ functions) with the $K=0$ functions. Table IV shows that the l-doubling parameter δ of the $|K|=2$ levels, which we defined by setting the f-e parity splitting equal to $\delta J(J+1)$, is on the order of $10^{-7}-10^{-8}$cm^{-1}.

The results in Tables II–IV further give rise to the following comments. States with $m_A=m_B=K=0$, i.e., $l_{\mathrm{HCN}}=l_{\mathrm{HCl}}=0$, have e parity. Hence, the lowest $K=0$ state of f parity is the state with $l_{\mathrm{HCN}}=-l_{\mathrm{HCl}}=\pm1$ at 352.2 cm^{-1} in which both the HCN libration and the HCl libration are excited. The same state, with energy 352.3 cm^{-1}, occurs with

TABLE III. Bound levels of HCN-H^{35}Cl for $|K|=1$: e levels for $J=1$ and band origins ν_0 relative to the ground level with $D_0=1091.3529$ cm^{-1}, rotational constants B, and l-doubling constants q; all quantities in cm^{-1}. Levels labeled with a and b are Fermi resonances; their quantum numbers v_s and $v_{b\mathrm{HCN}}$ are mixed.

v_s	$v_{b\mathrm{HCN}}$	$\lvert l_{\mathrm{HCN}}\rvert$	$v_{b\mathrm{HCl}}$	$\lvert l_{\mathrm{HCl}}\rvert$	e level	ν_0	B	$q\times10^4$
0	1	1	0	0	48.8792	48.7464	0.06646	1.82
0^a	3^a	1	0	0	125.9522	125.8166	0.06787	1.78
1^a	1^a	1	0	0	152.2532	152.1219	0.06570	1.59
0^b	5^b	1	0	0	200.5285	200.3888	0.06992	1.57
2^b	1^b	1	0	0	228.7618	228.6292	0.06646	2.65
1^b	3^b	1	0	0	252.8253	252.6937	0.06582	0.54
		1	0	0	276.4723	276.3301	0.07112	0.43
		1	0	0	302.3174	302.1745	0.06995	−27.40
0	0	0	1	1	311.8636	311.7342	0.06474	0.38
		1	0	0	323.8205	323.6891	0.06582	2.43
		1	0	0	349.5681	349.4342	0.06697	0.54
		1	0	0	353.7508	353.6104	0.07067	9.79
		1	0	0	375.4727	375.3320	0.07042	0.82
0	2	0	1	1	384.6177	384.4851	0.06629	−0.46
0	2	2	1	1	391.7104	391.5769	0.06668	−1.28
		1	0	0	393.6838	393.5520	0.06645	11.22

TABLE IV. Bound levels of HCN-$H^{35}Cl$ for $|K|=2$: e levels for $J=2$ relative to the ground level with $D_0=1091.3529$ cm^{-1} and l-doubling constants δ; all quantities in cm^{-1}. Levels labeled with a and b are Fermi resonances; their quantum numbers v_s and $v_{b\mathrm{HCN}}$ are mixed.

v_s	$v_{b\mathrm{HCN}}$	$\lvert l_{\mathrm{HCN}}\rvert$	$v_{b\mathrm{HCl}}$	$\lvert l_{\mathrm{HCl}}\rvert$	e level	$\delta\times 10^8$
0	2	2	0	0	94.3822	−1.4
0^a	4^a	2	0	0	168.8112	−0.7
1^a	2^a	2	0	0	199.7122	13.6
0^b	6^b	2	0	0	242.0339	0.8
2^b	4^b	2	0	0	272.3910	−9.6
1^b	2^b	2	0	0	300.4720	35.6
		2	0	0	318.6734	0.6
		2	0	0	343.0025	−16.0
0	1	1	1	1	353.2351	−11.9
		2	0	0	367.1671	22.6
		2	0	0	395.8086	
		2	0	0	395.9434	

e parity. This combination state has another component with $l_{\mathrm{HCN}}=l_{\mathrm{HCl}}=\pm 1$ and $|K|=2$ with both e and f parity. The energy of the latter component is 352.8 cm^{-1}.

Some levels, for example, the $K=0$ levels at 301.9 and 354.0 cm^{-1} in Table II, have anomalously large distortion constants D_J. These levels are perturbed by Coriolis interactions with nearby $|K|=1$ levels. The latter exhibit anomalously large l-doubling constants q, see Table III, for the same reason.

The Fermi resonances between the HCN librational modes with $v_{b\mathrm{HCN}}=2,4,6$ and $l_{\mathrm{HCN}}=0$ and the stretch modes with $v_s=1,2,3$ that we mentioned above are marked in Table II. The same type of resonances occur between the $|K|=1$ levels with $v_{b\mathrm{HCN}}=3,5$ and $l_{\mathrm{HCN}}=1$ and the levels with one quantum of stretch excited instead of each two HCN librational quanta, see Table III. And, again, between the $|K|=2$ levels with $v_{b\mathrm{HCN}}=4,6$ and $l_{\mathrm{HCN}}=2$ and the levels with one extra quantum of stretch for each two HCN librational quanta, see Table IV.

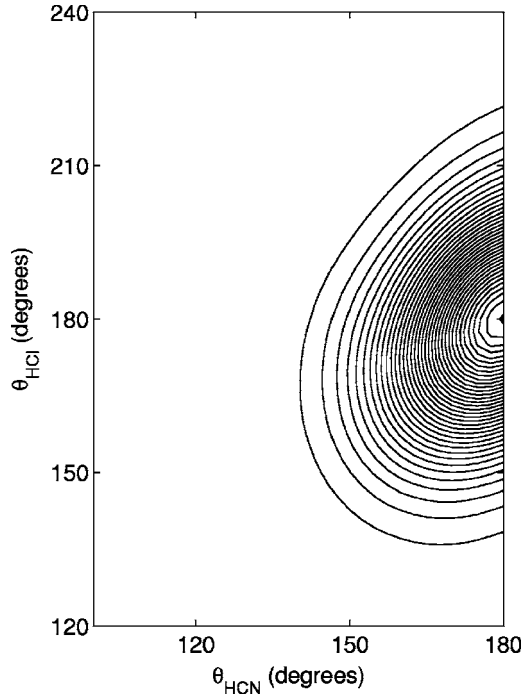

FIG. 5. Ground-state wave function, e symmetry, $K=0$. Cuts for $\phi=180°$ and $\phi=0°$ are combined as in Fig. 1; $R=7.4a_0$.

The wave functions of the HCN librational progression are displayed in Fig. 6, those of combinations of HCN and HCl librational states in Figs. 7 and 8. All of the characteristic nodes are clearly visible, although it is also clear that for the states of e parity the HCN libration involves some libration of the HCl molecule as well, and vice versa. A much better separation occurs for the states of f parity, where the orientation of the nodal planes is partly fixed by symmetry. The energies of the corresponding e and f states are very similar, however, even for $K=0$.

C. Isotope effects on the bound states

The results computed for different isotopomers of HCN–HCl are summarized in Table V. First we discuss the effect of substituting HCN by DCN, next that of replacing $H^{35}Cl$ by $H^{37}Cl$.

The frequency of the HCN libration shifts down from HCN–HCl to DCN–HCl by an amount of 3.34 cm^{-1}, i.e., by almost 7%. The downward shift expected in a harmonic model is 10%, proportional to the square root of the ratio of the rotational constants of DCN and HCN. The fact that the actual shift is smaller is probably due to the large amplitude of the librational mode giving rise to anharmonic effects. The HCl librational frequency is also affected by the HCN/DCN substitution, but only very slightly. It shifts up from HCN–HCl to DCN–HCl by 0.22 cm^{-1}. The rotational constant B becomes somewhat smaller. Partly this is an effect of the increased reduced mass of the complex, and partly it is caused by the average hydrogen bond length $R_0=7.848a_0$ of DCN–HCl being larger than $R_0=7.710a_0$ for HCN–HCl. The latter is caused by the smaller zero-point amplitude of the DCN libration in comparison with the HCN libration, leading to a more extended average linear structure of DCN–HCl. The intermolecular stretch frequency decreases by 2.3%, while the reduced mass ratio of DCN–HCl and HCN–HCl would give a decrease of only 1.0% in the harmonic approximation. The remainder should be ascribed to the effects of the increased average bond length and of anharmo-

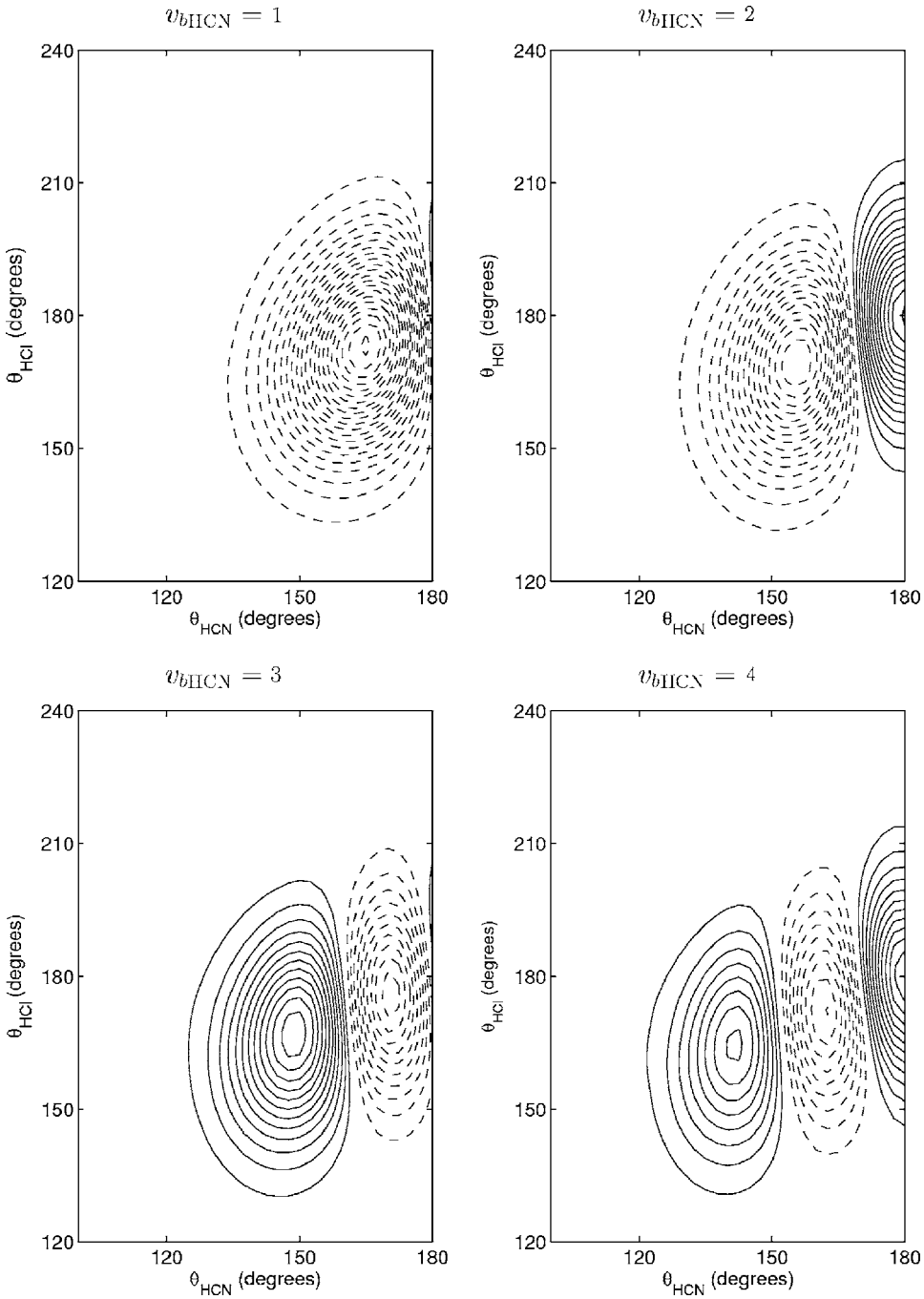

FIG. 6. HCN librational progression, wave functions of e symmetry at excitation energies of 48.8792, 84.1786, 125.9522, and 161.8786 cm^{-1} for $v_{b\mathrm{HCN}}=1$, 2, 3, and 4. States with even and odd v_b have $K=0$ and $K=1$, respectively. Cuts for $\phi=180°$ and $\phi=0°$ are combined as in Fig. 1; $R=7.4a_0$.

nicity. The change of the small l-doubling constant q is probably significant for the HCN libration. The value of q for the HCl libration is still smaller by an order of magnitude and will be rather unreliable, due to the fact that even the large angular basis which we used is not sufficient to converge the very small f-e parity splitting of the HCl libration excited level.

The shifts of the librational frequencies with the $H^{35}Cl$ to $H^{37}Cl$ substitution are extremely small. The fact that the HCN libration shifts only slightly when $H^{35}Cl$ is replaced by $H^{37}Cl$ may not be surprising, but for the HCl librational frequency the computed shift of about 0.007 cm^{-1} is smaller by more than an order of magnitude than the shift of 0.23 cm^{-1} expected from the ratio of the rotational constants of $H^{37}Cl$ and $H^{35}Cl$ in a harmonic model. We found the following explanation. Although the potential of HCN–$H^{37}Cl$ is the same as that of HCN–$H^{35}Cl$, the anisotropy of this potential for the libration of HCl is different, due to the shift of the center of mass of HCl. It is precisely this phenomenon that necessitated a re-expansion of the HCN–$H^{35}Cl$ potential in the bound state calculations of HCN–$H^{37}Cl$; see Sec. IV. We separately evaluated the effect of this change in anisotropy of the potential and the effect of the change of the mass and rotational constant of HCl in the kinetic-energy operator by repeating the HCN–$H^{37}Cl$ bound state calculations with the untransformed HCN–$H^{35}Cl$ potential. The results, where the shifts are merely caused by the change of the terms in the kinetic energy that depend on the HCl mass and rotational constant, are shown in the last column of Table V in parentheses. The lowering of the HCl librational frequency by

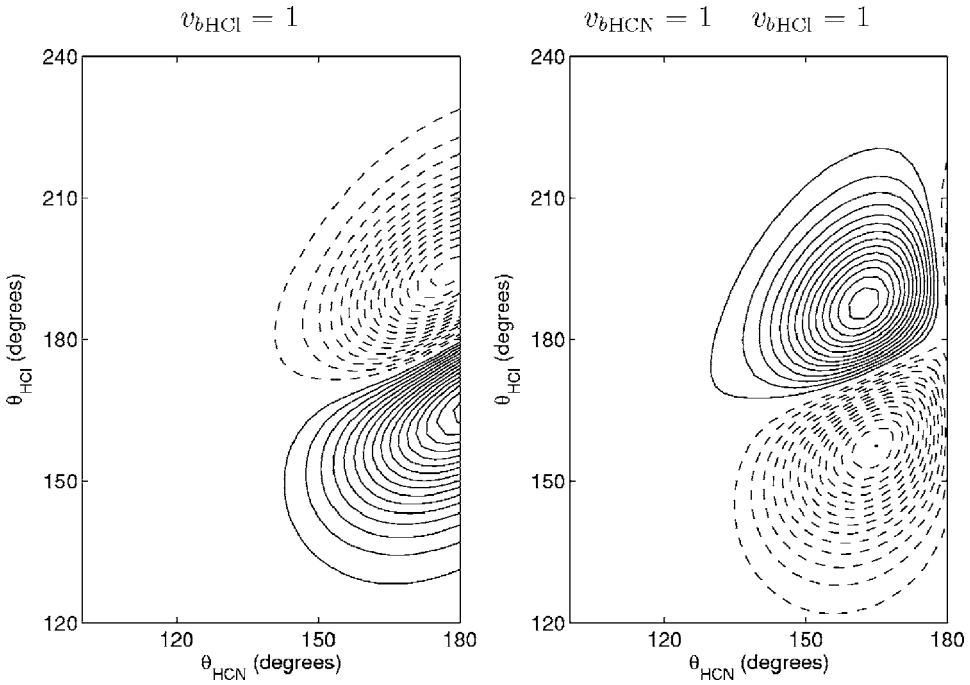

FIG. 7. HCl libration and HCN–HCl libration combination, wave functions of e symmetry at excitation energies of 311.8636 and 352.2988 cm^{-1} for $v_{b\mathrm{HCN}}=0$ and 1 with $v_{b\mathrm{HCl}}=1$. Even and odd values of total v_b correspond to $K=0$ and $K=1$, respectively. Cuts for $\phi=180°$ and $\phi=0°$ are combined as in Fig. 1; $R=7.4a_0$.

0.16 cm^{-1} is more normal now; the ratio of the rotational constants of $H^{37}Cl$ and $H^{35}Cl$ gives a lowering of 0.23 cm^{-1} in the harmonic approximation. Hence, the fact that the shift of the HCl librational frequency in the regular HCN–$H^{37}Cl$ calculation is so extremely small is caused by the near cancellation of two larger shifts: a downward shift from the effect of the Cl mass-dependent kinetic-energy terms and an upward shift from the increased anisotropy of the potential. The fact that this anisotropy has increased can be understood from the observation that the protruding hydrogen atom of HCl is further away from the mass center in $H^{37}Cl$ than in $H^{35}Cl$. The intermolecular stretch frequency shifts down by 0.8%, which is slightly less than the harmonic shift expected from the ratio of the reduced masses of HCN–$H^{37}Cl$ and HCN–$H^{35}Cl$. From the rotational constants B one derives that the average hydrogen bond length $R_0=7.710a_0$ of HCN–$H^{37}Cl$ is nearly the same as in HCN–$H^{35}Cl$.

D. Comparison with experiment and literature data

Our results may be compared in detail with the high resolution spectra of different HCN–HCl isotopomers measured by Larsen *et al.*[10] These spectra concern the HCl libration (or bend) mode, the band origin of which was found at 331.399 66 cm^{-1} for HCN–$H^{35}Cl$. We found a frequency of 311.73 cm^{-1} for this band origin, only 6% too low, which indicates that our potential surface is fairly accurate. The measured ground-state rotational constant B'' is

TABLE V. Computed properties of different HCN-HCl isotopomers (in cm^{-1}). All vibrational excitation energies from e levels with $J=1$.

	HCN-$H^{35}Cl$	DCN-$H^{35}Cl$	HCN-$H^{37}Cl$[a]
	Binding energy		
D_0	1091.35	1095.94	1092.02(1092.21)
	Vibrational frequencies		
HCN libration fundamental	48.7479	45.4074	48.7365(48.7576)
HCN libration overtone ($l=0$)	84.1812	79.4720	83.8659(83.8994)
HCl libration fundamental	311.7324[b]	311.9570[b]	311.7252[b](311.5727)
HCN+HCl libration combination	352.2987	349.6621	352.3126(352.1952)
intermolecular stretch	102.5989	100.1994	101.8278(101.8452)
	Ground-state rotational constant		
B	0.06564[c]	0.06206[c]	0.06418(0.06424)
	l-doubling constant $q\times10^4$		
HCN libration fundamental	1.82	1.30	1.74(1.73)
HCl libration fundamental	0.38[d]	0.07[d]	0.57(0.51)

[a]Values in parentheses computed with untransformed HCN-$H^{35}Cl$ potential.
[b]Experimental (Ref. 10) values of 331.399 66, 331.702 52, 331.3781 cm^{-1}.
[c]Experimental (Ref. 10) values of 0.066 999 18, and 0.063 300 0 cm^{-1}.
[d]Experimental (Ref. 10) values of 0.2946, and 0.2703 cm^{-1}.

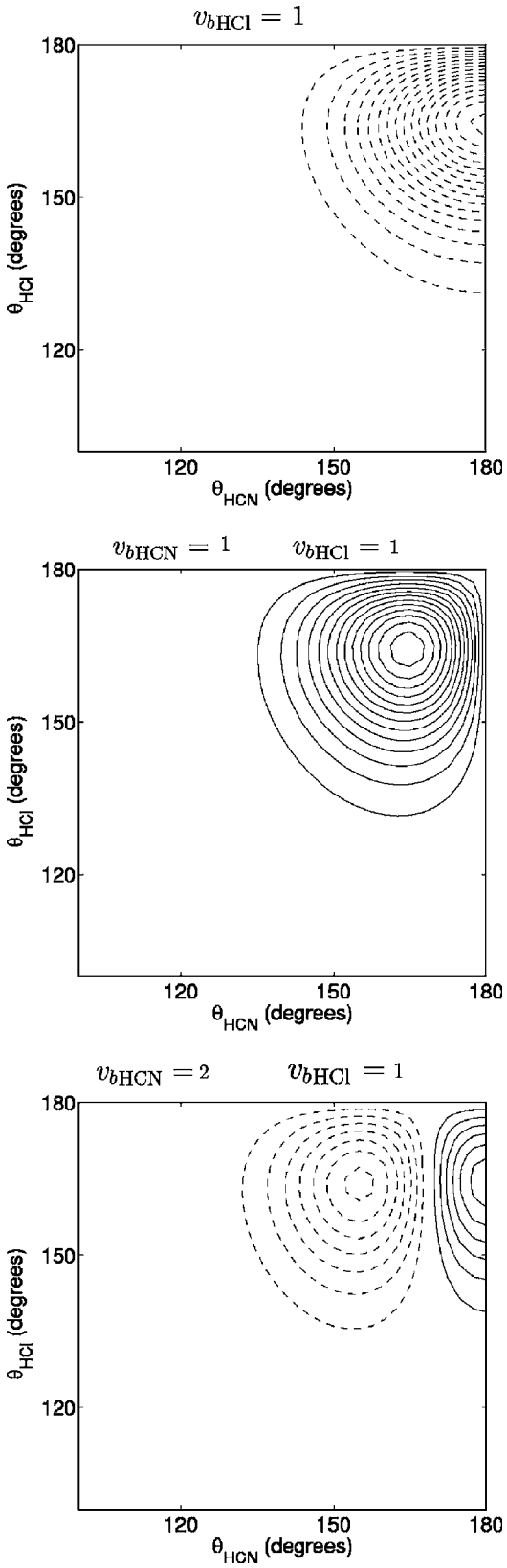

FIG. 8. HCl libration and HCN–HCl libration combinations, wave functions of f symmetry at excitation energies of 311.7342, 352.1834, and 384.6176 cm^{-1} for $v_{b\mathrm{HCN}}=0$, 1, 2 with $v_{b\mathrm{HCl}}=1$. Even and odd values of total v_b correspond to $K=0$ and $K=1$, respectively. Cuts for $\phi=90°$ and $R=7.4a_0$. The external rotation angle $\beta=90°$.

0.066 999 18 cm^{-1} and the distortion constant D_J'' is 0.1136×10^{-6} cm^{-1}, while we found $B''=0.065\,64$ cm^{-1} and $D_J''=0.1137\times10^{-6}$ cm^{-1}. The experimental ΔB value ($\Delta B=B'-B''$ and B' is the excited state rotational constant) is $-0.000\,979\,11$ cm^{-1}; we computed $\Delta B=-0.000\,920$ cm^{-1}. For all of these quantities there is good agreement between theory and experiment, which confirms the accuracy of the *ab initio* potential surface. Even the very small l-doubling constant q_6 of the HCl libration (the ν_6 mode) has the correct order of magnitude: we found $q_6=0.38\times10^{-4}$ cm^{-1}, the measured value is $q_6=0.2946\times10^{-4}$ cm^{-1}.

The shift of the HCl librational frequency with the substitution of HCN by DCN is 0.3029 cm^{-1}. We computed a shift of 0.22 cm^{-1}, in the same upward direction. Although the relative error is not small we consider the agreement as fairly good, given the indirect nature of the shift. The ground-state rotational constant B'' decreases by 0.003 70 cm^{-1} from 0.066 999 18 cm^{-1} for HCN–HCl to 0.063 300 0 cm^{-1} for DCN–HCl. The corresponding decrease of B'' from our calculations is 0.003 58 cm^{-1}, in very good agreement. The computed change in the q_6 value of the HCl libration is unrealistic, however, due to the difficulty of converging this very small quantity.

The measured frequency lowering of the HCl libration fundamental when $H^{35}Cl$ is replaced by $H^{37}Cl$ is 0.0216 cm^{-1}. Although the relative error between this shift and the computed shift of 0.007 cm^{-1} is not small, we conclude that the agreement is remarkable: both experiment and theory give a shift that is smaller by an order of magnitude than the harmonic model prediction of 0.23 cm^{-1} based on the ratio of the $H^{37}Cl$ and $H^{35}Cl$ rotational constants. With the aid of additional calculations we found the origin of this anomalously small shift. It is caused by a near cancellation of two larger shifts with opposite signs: one from the change of the HCl mass and rotational constant in the kinetic energy and one from the change of the effective anisotropy of the potential.

Also hot bands in which the HCl libration is excited from initial levels that correspond to the low-lying HCN libration fundamental and its overtones were reported in Ref. 10. The final levels in these transitions have the same HCN librational quantum numbers $v_{b\mathrm{HCN}}$ and l_{HCN} as the initial levels. From tentative assignments of the HCN–$H^{35}Cl$ spectrum it follows that the frequencies of the hot bands with $v_{b\mathrm{HCN}}=1$ and $v_{b\mathrm{HCN}}=2$ are redshifted with respect to the HCl libration fundamental by 5.2 and 10.1 cm^{-1}, respectively. The frequency that we computed for the HCN+HCl libration combination with $K=2$ is 352.8 cm^{-1} and the fundamental frequencies of the HCN and HCl librations are 48.7 and 311.7 cm^{-1}, respectively. Hence, the redshift (or anharmonicity constant) computed for the first hot band with $v_{b\mathrm{HCN}}=1$ relative to the HCl libration fundamental is 7.6 cm^{-1}. This anharmonicity constant would have been 8.1 cm^{-1} if we had taken the HCN+HCl libration combination with $K=0$. The measured value probably refers to the $K=2$ band. The computed frequency for the HCN overtone+HCl libration combination with $v_{b\mathrm{HCN}}=2$, $l_{\mathrm{HCN}}=0$, and $K=1$ is 384.5 cm^{-1} and the corresponding HCN overtone frequency is 84.2 cm^{-1}, so we obtain for the second hot band with

$v_{b\mathrm{HCN}}=2$ and $l_{\mathrm{HCN}}=0$ a redshift of 11.4 cm^{-1} relative to the HCl libration fundamental. The HCN overtone+HCl libration combination with $v_{b\mathrm{HCN}}=2$, $l_{\mathrm{HCN}}=2$, and $K=1$ has a frequency of 391.7 cm^{-1} and the corresponding HCN overtone frequency is 94.4 cm^{-1}, so the second hot band with $v_{b\mathrm{HCN}}=2$ and $l_{\mathrm{HCN}}=0$ has a calculated redshift of 14.4 cm^{-1}. The experimental shift of 10.1 cm^{-1} for the second hot band is believed to belong to the HCN libration overtone with $v_{b\mathrm{HCN}}=2$ and $l_{\mathrm{HCN}}=2$. The assignment of this hot band to the $l_{\mathrm{HCN}}=0$ component of the $v_{b\mathrm{HCN}}=2$ overtone is in better agreement with our calculations, but perhaps the use of the frequency for $K=3$ instead of the one computed for $K=1$ would have given a different result.

Frequencies of 53, 115, and 312 cm^{-1} for the HCN libration, intermolecular stretch, and HCl libration were obtained from harmonic calculations by Araújo and Ramos,[4] in fairly good agreement with our results from fully anharmonic and coupled four-dimensional calculations, see Table V. For the electronic structure calculations they used the MP2 method. Experimental estimates[7] for the level origins of the HCN libration (or bend vibration) and the intermolecular stretch vibration are 41 and 100 cm^{-1}. Also these values agree reasonably well with our computed HCN libration and intermolecular stretch frequencies of 48.7 and 102.6 cm^{-1}.

VI. CONCLUSION

We calculated a four-dimensional intermolecular potential energy surface for the HCN–HCl complex with rigid monomers with the use of the CCSD(T) method in an aug-cc-pVTZ basis. BSSE-corrected interaction energies were computed for 13 425 geometries. An angular expansion in terms of coupled spherical harmonics was fitted to these data with the aid of a combined interpolation/integration procedure; the dependence of the expansion coefficients on the intermolecular distance R was described by the reproducing kernel Hilbert space (RKHS) method. The global minimum in the potential with $D_e=1565$ cm^{-1} and $R_e=7.47a_0$ corresponds to a linear HCN–HCl hydrogen bonded structure with HCl as the donor. A secondary hydrogen bonded equilibrium structure with $D_e=564\mathrm{cm}^{-1}$ and $R_e=8.21a_0$ has a T-shaped geometry with HCN as the donor and the acceptor HCl molecule nearly perpendicular to the intermolecular axis.

This potential surface was used in a series of bound state computations for the isotopomers HCN–H^{35}Cl, DCN–H^{35}Cl, and HCN–H^{37}Cl with total angular momentum $J=0$, 1, 2 and spectroscopic parities e, f. The method used is a contracted DVR scheme in the intermolecular distance R, combined with a coupled channel approach in the internal angles $\theta_{\mathrm{HCN}}, \theta_{\mathrm{HCl}}, \phi$ of the complex and the Euler angles of the overall rotation. For the calculations on DCN–H^{35}Cl and HCN–H^{37}Cl, because of the shift of the monomer centers of mass, the potential of HCN–H^{35}Cl had to be re-expanded in a new set of internal Jacobi coordinates R', θ'_{HCN}, θ'_{HCl}, and ϕ'.

The bound states of HCN–HCl could be analyzed in terms of the approximate quantum numbers $v_{b\mathrm{HCN}}, l_{\mathrm{HCN}}$ and $v_{b\mathrm{HCl}}, l_{\mathrm{HCl}}$ of a linear polyatomic molecule with two internal librators, plus a quantum number v_s for the intermolecular stretch vibration. Also the quantum number $K=l_{\mathrm{HCN}}+l_{\mathrm{HCl}}$, which is simultaneously the projection of **J** on the intermolecular axis **R**, plays an important role in determining the character of the bound states. The shifts in the vibrational frequencies, rotational, and l-doubling constants caused by isotopic substitutions were discussed. The effects of replacing HCN by DCN are in line with predictions based on the mass and rotational constant ratios in a harmonic oscillator model. Replacing H^{35}Cl by H^{37}Cl gives seemingly anomalous effects, which could be understood after separating the kinetic mass effects from the effects of the modified anisotropy of the potential caused by the change of Jacobi coordinates. The results were compared with the recent high resolution spectrum of Larsen *et al.*[10] in the region of 330 cm^{-1} corresponding to the HCl libration. The agreement between theory and experiment is good, which confirms the accuracy of our HCN-HCl potential surface.

ACKNOWLEDGMENTS

Stimulating discussions with Dr. René Wugt Larsen are gratefully acknowledged. Dr. Gerrit C. Groenenboom is thanked for carefully reading the manuscript. One of the authors (G.S.F.D.) was financially supported by the Council for Chemical Sciences of the Netherlands Organization for Scientific Research (CW-NWO). One of the authors (B.F.) acknowledges support from the EU NANOQUANT RTN, Contract No. MRTN-CT-2003-506842 and by the Ministerio de Educacin y Ciencia and FEDER (Project No. CTQ2005-01076). One of the authors (H.K.) acknowledges computer time at the Danish Center for Scientific Computing.

[1] T. B. Pedersen, J. L. Cacheiro, B. Fernández, and H. Koch, J. Chem. Phys. **117**, 6562 (2002).
[2] J. L. Cacheiro, B. Fernández, T. B. Pedersen, and H. Koch, J. Chem. Phys. **118**, 9596 (2003).
[3] M. Havenith and G. Schwaab, Z. Phys. Chem. **219**, 1053 (2005).
[4] R. C. M. U. Araújo and M. N. Ramos, J. Braz. Chem. Soc. **9**, 499 (1998).
[5] C. Møller and M. S. Plesset, Phys. Rev. **46**, 618 (1934).
[6] A. C. Legon, E. J. Campbell, and W. H. Flygare, J. Chem. Phys. **76**, 2267 (1982).
[7] D. Bender, M. Eliades, D. A. Danzeiser, E. S. Fry, and J. W. Bevan, Chem. Phys. Lett. **131**, 134 (1986).
[8] P. A. Block and R. E. Miller, J. Mol. Spectrosc. **147**, 359 (1991).
[9] R. W. Larsen, F. Hegelund, and B. Nelander, Chem. Phys. **310**, 163 (2005).
[10] R. W. Larsen, F. Hegelund, and B. Nelander, Phys. Chem. Chem. Phys. **7**, 1953 (2005).
[11] K. Raghavachari, G. W. Trucks, J. A. Pople, and M. Head-Gordon, Chem. Phys. Lett. **157**, 479 (1989).
[12] K. Hinds and A. C. Legon, Chem. Phys. Lett. **240**, 467 (1995).
[13] G. Herzberg, *Spectra of Diatomic Molecules Molecular Spectra and Molecular Structure Vol. 1* (Van Nostrand, New York, 1950).
[14] A. van der Avoird, P. E. S. Wormer, and R. Moszynski, Chem. Rev. (Washington, D.C.) **94**, 1931 (1994).
[15] T. H. Dunning, J. Chem. Phys. **90**, 1007 (1989).
[16] R. A. Kendall, T. H. Dunning, and R. J. Harrison, J. Chem. Phys. **96**, 6796 (1992).
[17] D. E. Woon and T. H. Dunning, Jr., J. Chem. Phys. **98**, 1358 (1993).
[18] S. F. Boys and F. Bernardi, Mol. Phys. **19**, 553 (1970).
[19] Computer code DALTON, *a molecular electronic structure program, Release 2.0* (2005), see http://www.kjemi.uio.no/software/dalton/dalton.html.
[20] H. Koch, B. Fernández, and O. Christiansen, J. Chem. Phys. **108**, 2784 (1998).
[21] G. S. F. Dhont, J. H. van Lenthe, G. C. Groenenboom, and A. van der Avoird, J. Chem. Phys. **123**, 184302 (2005).

[22] G. W. M. Vissers, G. C. Groenenboom, and A. van der Avoird, J. Chem. Phys. **119**, 277 (2003).
[23] Computer code MATLAB *Version 6.5* (The MathWorks, Natick, Massachusetts, 2002).
[24] D. M. Brink and G. R. Satchler, *Angular Momentum*, third ed. (Clarendon, Oxford, 1993).
[25] T.-S. Ho and H. Rabitz, J. Chem. Phys. **104**, 2584 (1996).
[26] T.-S. Ho and H. Rabitz, J. Chem. Phys. **113**, 3960 (2000).
[27] A. van der Avoird, P. E. S. Wormer, F. Mulder, and R. M. Berns, Top. Curr. Chem. **93**, 1 (1980).
[28] J. F. Stanton, J. Gauss, and J. D. Watts *et al.*, Computer code ACES II, University of Florida, Gainesville, Florida, 1996.
[29] A. G. Maki, J. Phys. Chem. Ref. Data **3**, 221 (1974).
[30] F. C. DeLucia, P. Helminger, and W. Gordy, Phys. Rev. A **3**, 1849 (1971).
[31] G. C. Groenenboom and D. T. Colbert, J. Chem. Phys. **99**, 9681 (1993).
[32] E. R. Davidson, J. Comput. Phys. **17**, 87 (1975).
[33] G. C. Groenenboom, P. E. S. Wormer, A. van der Avoird, E. M. Mas, R. Bukowski, and K. Szalewicz, J. Chem. Phys. **113**, 6702 (2000).
[34] G. W. M. Vissers, L. Oudejans, R. E. Miller, G. C. Groenenboom, and A. van der Avoird, J. Chem. Phys. **120**, 9487 (2004).
[35] P. E. S. Wormer, J. Kłos, G. C. Groenenboom, and A. van der Avoird, J. Chem. Phys. **122**, 244325 (2005).
[36] R. L. DeLeon and J. S. Muenter, J. Chem. Phys. **80**, 3992 (1984).
[37] W. A. Sokalski and A. Sawaryn, J. Chem. Phys. **87**, 526 (1987).
[38] G. Maroulis and C. Pouchan, Theor. Chim. Acta **93**, 131 (1996).
[39] S. L. Hartford, W. C. Allen, C. L. Norris, E. F. Pearson, and W. H. Flygare, Chem. Phys. Lett. **18**, 153 (1973).
[40] E. W. Kaiser, J. Chem. Phys. **53**, 1686 (1970).
[41] G. Maroulis, J. Chem. Phys. **108**, 5432 (1998).
[42] F. H. de Leeuw and A. Dymanus, J. Mol. Spectrosc. **48**, 427 (1973).